Exploration of a polymer responsive potentiometric biosensor for the detection of flagella and whole cell of *Proteus mirabilis:* Proof-of-concept

M. Azizur R. Khan [a,b,1,], A. Cervellera-Dominguez [a,1], M. Goreti F. Sales [c] and Jordi Riu [a]*

[a]Department of Analytical and Organic Chemistry, Universitat Rovira i Virgili, C/ Marcel·lí Domingo s/n, 43007, Tarragona, Spain.

[b]Department of Chemistry, Jashore University of Science and Technology, Jashore-7408, Bangladesh.

[c]BioMark/CEMMPRE-ARISE, Department of Chemical Engineering, Faculty of Sciences and Technology, University of Coimbra, 3030-790, Coimbra, Portugal

1) equal first authors.

***** Correspondence

To whom correspondence should be addressed: *M. Azizur R. Khan,* Department of Chemistry, Jashore University of Science and Technology, Jashore-7408, Bangladesh. E-mail address: m.azizurrahman.khan@gmail.com, m.azizurrahman.khan@just.edu.bd, Tel: +880-242-142045, Ext. 212

Abstract

This work presents a novel biosensor based on molecularly imprinted polymers (MIP) to detect the flagella of *Proteus mirabilis* and describes experiments of the response to the whole bacterial cell. The MIP was obtained directly on the surface of gold electrodes, by electropolymerisation of pyrrole in the presence of *Proteus mirabilis* flagella, using cyclic voltammetry. The imprinted polymer matrix was then treated with trypsin to enzymatically digest the flagella and expose the complementary cavities that served as selective recognition sites.

The performance of the electrodes prepared with the MIP materials and the corresponding controls was evaluated by potentiometric assays in HEPES buffer. This was performed for the flagella of *Proteus mirabilis* and the whole cell of the bacterium. The limit of detection (LOD) for flagella was 0.251 µg/mL when using the MIP and 0.758 µg/mL when using the control non-imprinted polymer (NIP). The imprinting factor (IF) demonstrated concentration-dependent enhancement of specific binding, with IF values of about 2.05 at 11.10 ng/mL, 7.30 at 111.10 ng/mL, and 13.60 at 311.10 ng/mL. Additionally, the slope of the NIP calibration curve was found to be lower than that of the MIP, further confirming that the sensitivity arises from the imprinted cavities. To confirm the preference of the material for the flagella, selectivity studies were performed against other non-target proteins, including glucose oxidase, *Staphylococcus aureus* protein A and bovine serum albumin.

Overall, the results showed good sensitivity and high selectivity for *Proteus mirabilis* flagella, emphasising the promising potential of this MIP-based sensor for the rapid and cost-effective detection of bacterial proteins. However, the detection of the whole cell under the tested conditions remained limited. This could be due to the cell's ability to move, as it has flagella and its driving force for movement is likely higher than the binding affinity for the MIP, which relies only on non-covalent bonds.

Keywords: Screen-printed electrode; Electropolymerization; Molecular imprinted polymer; Potentiometric biosensor; Flagella from *Proteus mirabilis*; Whole cell of bacterium

1. Introduction

Proteus mirabilis is an important bacterium in terms of food safety and spoilage [1]. It breaks down proteins present in food, causing unpleasant odours/tastes, which is particularly important in protein-rich foods such as meat [2,3]. The presence of *Proteus mirabilis* can also indicate unhygienic conditions in food processing, as the bacterium can form biofilms on equipment used for food processing [4,5]. Thus, monitoring and control of these bacteria in food production and processing is crucial to ensure food safety, prevent spoilage and reduce the risk of foodborne illness. This usually involves microbiological testing, which in a routine basis may involve culture-based methods for increasing the detection capacity [6,7]. These methods are typically linked to low sensitivity, unable to provide a quick answer, in time of implementing effective corrective measures that could eliminate/prevent further food contamination. Despite the great advances in the literature related to these methods, there are key cornerstones that remain to be solved, mostly related to (a) the complexity and diversity of the food matrices; (b) the randomly distributed pathogen in the sample and its low concentration levels; (c) possible collapse of the pathogen during processing; (d) the presence of bacteria from the normal microbiota; and (e) the timing between sampling and collection [8,9]. In addition, some common bacterial biochemical test such as Polymerase Chain Reaction (PCR) [10] and DNA sequencing [11] provide high specificity, Enzyme-Linked Immunosorbent Assay (ELISA) [12] is suitable for screening. But, those techniques require expensive natural receptors like antibody or DNA, costly equipment, high laborious time and specialized expertise.

One of the strategies reported in the literature enables quick and local responses signalling the presence of bacterial pathogens involves the use of biosensors [13–16], which are small compact devices that contain biorecognition and transduction elements in a single device. The biorecognition element is responsible for the selective binding of the target compound, and it can be of natural origin, as antibodies or enzymes, or of synthetic origin, as nucleic acids, aptamers or other biomimetic materials. The transduction scheme is mostly electrochemical (as for the glucose monitoring in diabetes) [17] or optical (as for the colorimetric urine strips) [18].

One of the emerging fields in terms quick and low-cost detection of bacteria is the use of molecularly imprinted polymer (MIP) materials as biorecognition elements [19–21]. MIPs are synthetic polymers planned to mimic the behaviour of antibodies (biomimetic biorecognition elements). They are obtained by imprinting technology, in which monomers and template (target

compound) are brought together to form a self-arranged complex. Upon addition of cross-linkers and monomers, a radical polymerization leads to the formation of a 3D network where the template is entrapped. The template is then removed, creating free binding sites that hold complementary shape and functionalities to the template [22–25]. Overall, MIPs are considered robust and advantageous molecular recognition elements, capable of acting like natural recognition entities, such as antibodies and biological receptors [26]. When the template of the imprinted template is of large size and complex structure, which is the case of a whole bacterium, a fraction of the template can be imprinted. Herein, the most suitable approach seemed to be the use of a fraction of the bacteria, using the *Proteus Mirabilis'* flagella, which is a lash-like appendage that is on the cell. The positioning of the external proteins of the cell is also variable from cell to cell, which makes the population of same bacteria highly heterogenous in terms of a 3D mould. Bacteria can undergo flagellar shedding due to various environmental stresses, such as changes in the environment or leading to the detachment of flagella from the cell body [27,28]. Detached flagella, primarily composed of flagellin proteins, can serve as valuable biomarkers for bacterial presence and identification [29].

As far as we know, there is a single MIP material assembled for *Proteus Mirabilis* flagella reported in the literature, using phenol monomers and in-situ electropolymerization [30], with electrochemical impedance spectroscopy (EIS) and square wave voltammetry (SWV) employed for the target detection. However, EIS and SWV-based detection process is hindered by a prolonged response time when transitioning between different target concentrations. In addition, while the use of phenol as monomer allows establishing intense hydrogen and electrostatic interactions with the imprinted compound, the polymeric network so generate has non-conductive features. This may hinder the electrical signal generated by electrochemical systems, but its impact may be controlled by the thickness of the polymeric film. In alternative, conductive polymers may be employed, such as polyaniline, polythiophene, polythylenedioxythiophene [31–34]. Among conductive polymers, polypyrrole (PPy) has been widely used for electrochemical sensing [31,35] , offering several advantages in terms of simplicity and recognition ability. However, the conductivity of polyphenol is 1.2×10^{-4} $S \cdot cm^{-1}$ [36], whereas polypyrrole exhibits significantly higher conductivity, approximately 10^{5} $S \cdot cm^{-1}$ [37] in thin-film form.

About the transduction scheme, the use of potentiometric-based systems is also preferred. In comparison to other electrochemical approaches, potentiometry introduces simplicity and low-cost, while allowing short response time and high sensitivity [38]. The most widely used potentiometric sensors are ion-selective electrodes (ISEs). In these, the sensing layer of ISEs is the ion-selective membrane that contains as biorecognition element an ionophore, which when the target compound exists in an ionic form can be a MIP material [39]. Traditionally the fabrication of the ion-selective membrane involves the mixing of the ionophores with suitable additives and/or with plasticizers to fabricate the cocktail membrane that will be deposited over the electrode surface [40–42]. The main drawback of this process is its time-consuming nature and the difficulty in controlling the thickness of the sensing layer, which may question reproducibility and the upscaling of the fabrication process. This procedure may be simplified by a direct preparation of the sensing system on an electrochemical set-up.

Furthermore, in this proof-of-concept study, both lipophilic salts and the conditioning step were intentionally omitted to evaluate the intrinsic performance of the MIP-FPM-based sensor in its simplest form. While lipophilic salts (e.g., potassium tetrakis(4-chlorophenyl)borate, KTpClPB) are commonly used in conventional ISEs to enhance membrane conductivity and stabilize the phase boundary potential, their inclusion in MIP-based systems could introduce non-specific ionic pathways, potentially compromising selectivity. In addition, in flexible or non-PVC matrices, these salts may leach over time, reducing stability. Similarly, although conditioning is important in traditional ISMs to establish membrane/solution equilibrium, its effect in MIP-FPM matrices is less predictable. Excluding conditioning allows direct assessment of the sensor's unconditioned performance, which is particularly relevant for point-of-care and disposable applications.

Thus, this work describes the development of a new MIP material for detecting flagella from *Proteus Mirabilis* that is PPy-based, applied in a potentiometric transduction. As a novelty in terms of potentiometry development, the sensing layer of the MIP-based sensor was directly fabricated on gold-screen printed electrodes (Au-SPEs), yielding a plasticizer-free architecture that departs from conventional potentiometric sensor designs. The fabrication of the overall system is described, optimized and characterized, with regard to the main analytical features. Application is also tried out for detecting the flagella and the whole cell.

2. Experimental

2.1. Equipment and instrumentation

High-input impedance voltmeter (1015 Ω), model EMF-16 Lawson Laboratories Inc (Malvern, PA, USA). Double junction standard commercial reference electrode (Ag/AgCl/KCl 3 M) containing a 1 M LiAcO electrolyte bridge, type 6.0729.100, Metrohm AG (Herisau, Switzerland). The electrochemical measurements were conducted with a potentiostat/galvanostat from Metrohm Autolab and a PGSTAT302N (Utrecht, The Netherlands), equipped with a FRA module and controlled by Nova software. The Au-SPEs were purchased from DropSens (Oviedo, Spain), and composed by a working electrode made of gold, a counter electrode made of gold and a reference electrode made of silver (electrical contacts were also made of silver). The diameter of the working electrode (WE) was 4.0 mm. The Au-SPEs were connected to a portable switch box, also from DropSens (DRP-DSC), allowing their interface with the potentiostat/galvanostat. Fourier transform infrared spectroscopy (FTIR) measurements were performed using a Thermo Scientific Smart iTR Nicolet iS10, coupled to SAGA smart accessory, also from Thermo Scientific (Waltham, USA). Transmission electron microscope (TEM), Jeol 1011, was from Japan.

2.2. Reagents and solutions

All chemicals were of analytical grade and water was de-ionized or ultrapure Milli-Q laboratory grade. Sulfuric acid (98%), potassium hexacyanoferrate III, potassium hexacyanoferrate II trihydrate, sodium acetate anhydrous, trypsin, pyrrole (98%), 2-(*N*-morpholino)ethanesulphonic acid monohydrate 98% (MES), bovine serum albumin (BSA), protein A from *Staphylococcus aureus* (PA), glucose oxidase (GOx), 4-(2-hydroxyethyl)-1-piperazineethanesulfonic acid (HEPES), tris(hydroxymethyl)aminomethane and potassium chloride (KCl) were from Sigma Aldrich. The MES buffer (1.0×10^{-2} mol/L, KCl 0.1M, pH 5.0) was used for the template molecule immobilization onto the WE of Au-SPE and Potassium ferro/ferricyanide probe solution preparation. Flagella from *Proteus mirabilis* (FPM) was obtained from the Department of Microbiology, University of Barcelona. Stock solutions of 1.22×10^{-5} mol/L flagella from *Proteus mirabilis* (FPM) were prepared in TRIS buffer (6.67×10^{-4} mol/L, pH 7.8) and stored at –20˚C. Standards were obtained by accurate dilution of the previous

solution in HEPES buffer (1.0×10^{-4} mol/L, variable pH 5, 7.3 or 8.5) depending on the applications. TRIS buffer (5.0×10^{-2} mol/L, $CaCl_2$ 1.0×10^{-3} mol/L pH 8.0) was used for trypsin solution preparation. The selectivity study was made in the HEPES (1.0×10^{-4} mol/L, pH 7.3) buffer using BSA, PA and GOx.

The bacterial culturing media tryptic soy broth (TSB) and tryptic soy agar (TSA) were purchased from Becton, Dickinson and Company (Sparks, USA), and they were prepared according to companies' provided indications. These non-selective media were used in the counting and cultivation of pure strains of *Proteus mirabilis* (PM).

2.3. Electrochemical synthesis of molecularly imprinted (MIP) and non-imprinted polymer (NIP) films

Prior to the electropolymerization, the Au-SPEs electrodes were cleaned with ethanol followed by electrochemical cleaning with 0.5 M H_2SO_4 (Cyclic Voltammetry, CV, from −0.2 to 1.2V, 15 cycles at a scan-rate of 50 mV/s). Then FPM were deposited at the working area of the Au-SPE: 10 µL of 200 µg/mL FPM solution prepared in MES buffer was exposed to the working area of the electrodes for 30 minutes at room temperature and gently washed with Milli-Q water. The immobilization was based on spontaneous physisorption of FPM onto the gold surface, a phenomenon well documented in the literature—for example; proteins like antibodies have been shown to irreversibly adsorb onto gold nanoparticles [43], forming stable layers that resist removal even after washing. However, 75µL of pyrrole solution (1×10^{-3} M) in acetate buffer (1×10^{-2} M, pH 5.0) was placed to cover the three electrodes and polymerization was performed by CV from -0.2 to 1.2 V (scan rate 0.05V/s, 15 CV cycles was found to be the optimal). Nonetheless, we took deliberate steps to ensure consistent polymerization conditions across all electrodes. Drawing on our previous experience in MIP fabrication, we employed a low concentration of pyrrole (1×10^{-3} M) in acetate buffer without additional salt to achieve a slower and more controlled deposition rate, thereby promoting uniform film formation. Flagella were removed by adding trypsin (500 µg/mL in TRIS buffer, 37^{O}C, and 2.5 h) and by the subsequent electrochemical cleaning in MES buffer (10 CV cycles from -0.6 to 1V, scan rate 50 mV/s). The fabrication of the MIP-based biosensors is schematically presented in **Figure 1.**

In parallel, non-imprinted polymers (NIPs) were synthesized in a similar mode, but without the presence of FPM.

2.4. Electrochemical characterization of the films

The polymer growth and the surface characteristics of MIP and NIP-films were followed by CV, electrochemical impedance spectroscopy (EIS) and squared-wave voltammetry (SWV). The redox probes in all CV and EIS measurements were 5.0 mmol/L $[Fe(CN)_6]^{3-}$ and 5.0 mmol/L $[Fe(CN)_6]^{4-}$ prepared in MES buffer (1.0×10^{-2} mol/L, KCl 0.1M, pH 5.0). In CV assays, the potentials ranged from –0.5 to +0.7 V with a scan rate of 50 mV/s. In EIS, an open circuit potential was set using a sinusoidal potential perturbation of 0.01 V amplitude and 50 frequency values logarithmically distributed over a frequency range of 0.1–100 kHz. In SWV the potential range was from –0.1 to 0.6 V.

2.5. Potentiometric measurements

In the case of potentiometric measurements, the working electrode was the gold electrode of the Au-SPE (which contained the MIP/NIP materials), tested against the standard commercial reference electrode (Ag/AgCl/KCl 3 M). The working electrode was stabilized in blank HEPES buffer at a fixed pH before starting the calibration. All the potentiometric measurements for FPM detection were carried out at room temperature and in stirred solutions. Electromotive force (EMF) values of each electrode were measured in HEPES buffer (1.0×10^{-4} mol/L) in fixed pH (5.0, 7.3 or 8.5). The best performance of the sensors at the calibration stage was found at pH 7.3 and these results are presented herein. For the detection of *Proteus mirabilis*, the potentiometric measurements were conducted using sterilized HEPES buffer, pH 7.3.

3. Results and discussions

3.1. Electrochemical imprinting

The typical cyclic voltammograms recorded during the MIP and NIP formation by electropolymerization are shown in **Figure 2A**, conducted on Au-SPEs that have high metallic conductivity [44]. The first voltammogram of the NIP corresponded to only pyrrole in acetate buffer presented two oxidation peaks, one at ~0.7V (of higher current intensity) and another at

~1.0V (of smaller intensity). The electropolymerization of pyrrole can lead to the formation of diverse structures, as reported in [45], in which two oxidation peaks are also a possibility. In addition to this, the polymerization was conducted in acetate medium, on a surface that was in contact with MES buffer (used at the FPM deposition stage, which in the MIP corresponded to incubation in MES), which are very specific conditions. However, the potential shift toward a higher anodic value observed during the first scan cycle of the MIP electropolymerization can be attributed to the hindered diffusion of pyrrole monomers caused by the presence of the FPM template. The FPM molecules, occupying specific recognition sites during polymer growth, likely reduce the accessibility and local mobility of pyrrole near the electrode surface. As a result, a higher overpotential is required to initiate polymerization, leading to the observed shift. In contrast, the NIP, lacking such a template-induced steric barrier, exhibits no significant shift in the oxidation potential during its first cycle, supporting the assertion that the shift is template-dependent. This behavior indicates that the presence of the FPM template plays a role in shaping the polymerization conditions.

In addition, the first oxidation peak was significantly reduced in subsequent voltammograms, which can reflect the small reduction peak observed in the reversed cycle, when compared to the oxidation peaks. As the overall current decreased upon consecutive cycling, the formation of the polymer on the electrode surface was confirmed, although not having conductive features (due to the specific conditions in which the polymerization took place).

Considering the MIP materials, only one oxidation peak was evident, at ~0.9 V. This could correspond to the shift of the first oxidation peak observed in the NIP to higher potential, in which the second oxidation peak would be covered by the capacitance current observed, due to the presence of FPM before starting polymerization. In alternative, a single oxidation peak could also have been observed, as the conductivity features of the electrode surface were limited, due to the presence of the flagella. As in the NIP, voltammograms of the MIP showed decreasing currents from the 1st cycle to the 9th cycle, indicating the deposition of a non-conductive polymer onto the electrode surface (although not as insulating as polyphenol). This was confirmed by the disappearance of the redox peaks of the ferro/ferricyanide probe with respect to the clean Au-SPE (**Figure 2B**). All these considerations around the peak shift require however

further studies around the redox species being formed in time and within the potential ranged at the electrode surface.

Comparing with the NIP, the anodic oxidation of pyrrole in the MIP displayed lower current intensities, which was an outcome of the presence of FPM before the electropolymerization stage. Moreover, the decreasing trend of the current in consecutive voltammograms was lower in the MIPs, indicating a lower polymer growth. This was correlated to the presence of the flagella at the electrode surface, blocking the access of pyrrole to the electrode and thereby hindering the formation of the radical species that are responsible to sustain the polymer growth.

3.2. EIS and SWV-based characterization

EIS and SWV were also employed for the characterization of the polymer films (**Figure 2C-D**). Typical EIS data of the MIP and NIP-films before and after the template removal is shown in **Figure 2C**, in the form of Nyquist plots and fitting values to the equivalent Randles circuit. In this, the semicircles observed at high frequency region indicated a charge-transfer controlled process. The diameter of this semicircle is equal to the charge-transfer resistance, R_{ct}, which governs the electron-transfer kinetics of the redox-probe at the electrode interface [46]. The linear behavior was observed at the low frequency range and exposed a diffusion-controlled mass-transfer process [47], represented by the Warburg element (W). Overall, the electrical circuit in EIS is composed of a resistor element (solution resistance, R_s) in series with one parallel circuit comprising a charge transfer resistance, Rct, with a Warburg element (W) and a double layer capacitance, C_{dl} (inset of **Figure 2C**) [48–50].

Table 1 presents the summarized data from the EIS-based characterization conducted before and after the template removal treatment, followed by a detailed explanation.

Table 1: Summarized data of EIS-based characterization

Material	R_{ct}			% of signal decay after template removal
	Clean Au-SPE	After polymerization	After the treatment for template removal	
MIP	0.15 kΩ	16.7 kΩ	1.8 kΩ	89.0%

NIP	9.8 kΩ	2.6 kΩ	73.5%

The polymerization contributed to a huge increase in the R_{ct} value of the clean electrode, which confirmed the formation of a polymeric compound at the surface of the electrode that does not hold conductivity features. The R_{ct} increased much more in the MIP (16.7 kΩ) than in the NIP (9.8 kΩ), which was expected considering the presence of FPM at the surface on the MIP, combined with the formation of a PPy in both surfaces (the formation of the polymer occurred in a lower extent in the MIP when compared to the NIP, due to the presence of the protein).

FPM was removed from the polymer network by the proteolytic action of trypsin. For comparison purposes, both MIP and NIP materials were incubated in the enzyme solution and after subject to electrochemical cleaning. In general, both R_{ct} values of MIP and NIP decreased significantly, down to 1.8 and 2.6 kΩ, respectively. As expected, this decreasing was more intense in the MIPs (89.0%) than in the NIPs (73.5%). In the case of MIPs, this decreasing rate involved two factors: (i) the removal of the template (FPM) and (ii) the elimination of non-bound monomers and/or oligomers, with the possibility of some polymer material loss. In contrast, for the NIP, only the latter factor is relevant since no FPM was incorporated during polymerization. The relative contribution of both (i) and (ii) can only be considered upon analyses of the absolute terms; one could say that the impact of the removal stage in (ii) corresponded to 7kΩ and in (i+ii) corresponded to ~15kΩ, meaning that about 50% of the signal decrease could be assigned to the loss of materials within the NIP membrane. Overall, the SWV data obtained in parallel (shown in **Figure 2D**) is consistent with EIS data. Importantly, the recovery of the peak current after FPM removal is highly evident in the case of the MIP.

3.3. FTIR-based characterization

FTIR analysis was performed for both MIP and NIP; however, the spectra appeared is identical (**Figure S1** Supplementary Information). This similarity is expected, as both polymers are synthesized from the same functional monomers and cross-linker, and the template protein (trypsin) is not covalently incorporated into the polymer backbone. Consequently, FTIR cannot provide clear differentiation between MIP and NIP. Nonetheless, the obtained spectrum confirms that the overall chemical structure of the polymer remains intact after template removal, indicating that trypsin does not alter the polymer framework.

3.4. Analytical performance of the sensors for the detection of flagella

Figure 3 shows the potentiometric performance of the sensors against increasing concentrations of FPM. As the analytical application is intended for bacterial infections, HEPES buffer solutions were employed herein, at ~pH of 7.3. In general, both devices (MIPs and NIPs) showed no response at lower concentration of FPM, below 11.1 ng/mL.

The MIP displayed a slight EMF decrease when the concentration of FPM was of 0.111 µg/mL. This decrease was the first EMF change that was clearly more intense than the random fluctuation of the blank or the readings of solutions with lower concentrations of FPM. For the same concentration of FPM, the EMF of the NIP remained unchanged. This is a typical behaviour of potentiometric systems with protein-based ion-selective electrodes with MIPs [51], confirming the higher binding capacity of the MIP than the NIP to capture FPM.

For concentrations higher than 0.111 µg/mL, the EMF of the MIP changed more intensely, keeping the same negative trend. This trend was near to a linear behaviour against log concentration of FPM, as may be seen in **Figure 3B**. The NIP also changed the EMF values in a negative trend, which confirmed the negative charge of FPM, but the magnitude of the EMF change was lower than in the MIP. This behaviour signalled the non-specific binding of FPM to the NIP (with only PPy), which is also typical in potentiometric systems with imprinted polymers. Overall, one could assume that the linear response trend in the MIP-devices was from 0.311 to 2.561 µg/mL while in case of NIP was from 0.811 to 2.561 µg/mL.

The method for determining the limit of detection (LOD) in potentiometric ion-selective electrodes (ISEs), is globally established by the International Union of Pure and Applied Chemistry (IUPAC). According to IUPAC guidelines, the LOD is defined as the concentration at which the extrapolated linear segments of the calibration curve intersect [52]. This approach is commonly referred to as the "cross point method". However, according to IUPAC method, the limits of detection (LODs) were 0.251 µg/mL and 0.758 µg/mL for MIP and NIP-devices) respectively. The response time was between 12 s and 15 s for both MIP and NIP-devices (inset of **Figure 3A**).

Furthermore, the calibration curve at the higher concentration range was constructed using four representative points for MIPs and three points for NIPs, showing clear linearity (R^2 = 0.91 for MIP and 0.97 for NIP) and demonstrating the feasibility of the MIP-based sensing strategy, where the MIP exhibited higher responses than the NIP **(Figure 3B)**. The low R-squared obtained is likely correlated to the intrinsic variability of the flagella, a biological material that is being used in this work as standard solution. Still, at lower concentrations, the MIP also produced measurable responses, confirming its sensitivity across the full range. Across both lower and higher concentrations, the MIP consistently showed smaller error bars than the NIP, highlighting its superior reproducibility and reliability. To further enhance calibration accuracy and statistical confidence, additional concentration points will be incorporated in follow-up investigations.

In addition, at lower concentrations, the MIP response was clearly distinguishable from the NIP, indicating minimal non-specific interactions in this range. At higher concentrations, some degree of non-specific binding was evident in the NIP, which is a common observation in protein-imprinted systems owing to the size and heterogeneous surface characteristics of proteins. Nevertheless, the MIP consistently exhibited higher and more reproducible responses across all tested concentrations. In addition, the calculated imprinting factor (IF) increased with concentration, further supporting the presence of specific recognition sites introduced by the imprinting process.

The imprinting factor (IF), calculated as the ratio of the MIP response to the NIP response, reflects the efficiency of cavity formation. Expressed as absolute values, the IF is approximately 2.05 at 11.10 ng/mL, 7.30 at 111.10 ng/mL, and 13.60 at 311.10 ng/mL, showing a clear concentration-dependent enhancement of specific binding. These results confirm that the MIP possesses well-formed recognition sites capable of selectively interacting with the target analyte. However, we acknowledge that relatively low imprinting factors at low concentrations of FPM limit the applicability of the sensor to high-concentration screening.

The negative EMF trend was related to the detection of negatively charged species, meaning that the proteins of the flagella used as standard were negatively charged under pH 7.3. Although unknown, the overall degree of protonation of each FPM unit was likely high, considering the small slope obtained in the calibration of the MIP (~9.56 mV/decade concentration). This was consistent with the operation of the flagella, which in bacteria relies on a proton flux motor,

making the proteins highly negative in terms of charge. The slope of the NIP (~6.65 mV/decade concentration) was lower than that of the MIP, which once more confirmed the higher affinity of the FPM for the MIP material, thereby supporting the existence of selective binding positions. The inherent response of the NIP is an outcome of the non-specific binding of the protein to PPy, which is common in potentiometric sensing with imprinted materials. Although the present study demonstrates promising analytical performance, repeatability assessments need to be considered in future studies to further establish the reproducibility and robustness of the sensor.

3.5. Regeneration of the sensors

Sensors were regenerated by employing the same protocol used for removing the template at the fabrication stage, in which the electrodes were subject to trypsin action followed by electrochemical cleaning EIS was employed to observe the surface characteristics of the MIP and NIP films before and after regeneration. After completion of the calibration, the R_{ct} value increased in both devices (MIPs 53.75 kΩ, NIPs 12.42 kΩ), with the MIPs showing a higher increment than NIPs (**Figure S2A** Supplementary Information). This increase in R_{ct} after calibration may reflect a combination of specific and non-specific interactions with the analyte, rather than indicating solely a higher binding capacity of the MIP layer.

After regeneration of the resulting surfaces, the R_{ct} value of both MIP and NIP-devices significantly decreased (**Figure S2B** Supplementary Information), down to ~810Ω in the MIP or to ~790Ω in the NIP. This R_{ct} values was lower than the ones corresponding to the first FPM removal, meaning that some additional polymeric network could have been lost or that the ionic content within the polymeric pores of the polymeric network was higher due to the consecutive incubations in electrolyte solutions. This last possibility is more consistent with the fact that MIP and NIP had similar R_{ct} values.

3.6. Selectivity

Selectivity is a critical parameter in the design and development of chemical sensors, particularly for complex biological samples where multiple biomolecules may be present. A

highly selective sensor ensures that the target analyte can be accurately detected without interference from other substances, thereby improving the reliability, accuracy, and clinical applicability of the device.

In this study, selectivity was evaluated using a separated-solution-based approach in which the electrochemical signal was first recorded for a fixed concentration of FPM (311.10 ng/mL). Subsequently, the signal responses were measured separately for the potentially interfering proteins—BSA, PA, and GOx—each at 58 times higher concentration (18.11 µg/mL) than FPM. These were selected as model interfering proteins for this proof-of-concept study. The possibility of testing rod-shaped proteins could have been interesting for checking the ability of the MIP to establish a spatial recognition of the target, but there is no nanostructure that we know of holding similar electrostatic features to the flagella.

The normalized responses of MIPs and NIPs are presented in **Figure 4**. Normalization was carried out by calculating the potential change (ΔE) for each protein (both MIPs and NIPs) and dividing it by the maximum potential change observed for FPM with MIPs, which elicited the highest response among all tested proteins. The MIP sensor exhibited a markedly stronger signal in response to FPM, whereas negligible responses were recorded even at high concentrations of BSA, PA, and GOx (**Figure 4A**). This pronounced difference in signal intensities underscores the high selectivity of the fabricated MIP sensor for FPM. These results clearly demonstrate the high selectivity of the fabricated MIP sensor toward FPM.

Figure 4B shows the NIP responses to FPM and the non-target proteins BSA, PA, and GOx. Although the response of NIPs to FPM (Figure 4B) was much lower than that of MIPs (Figure 4A); the relative responses of NIPs to FPM and non-target proteins were comparable. This indicates that, unlike MIPs, NIPs lack selectivity, an outcome that is consistent with the absence of imprinting cavities.

The ability of the MIP sensor to selectively recognize FPM even in the presence of a high excess of other proteins highlights its potential application in real-world biological and environmental monitoring, where selective detection is paramount for accurate diagnostics and analysis.

3.7. Detection of Proteus mirabilis

PM bacterial flagella were detected because imprinted materials perfectly preserve the size and shape of the target flagella from *Proteus mirabilis.* As a proof of concept, MIPs created by imprinting of flagella from *Proteus mirabilis* can have the ability to capture and detect the whole *Proteus mirabilis* cell since the outer surface of *Proteus mirabilis* contains those flagella. The images of the whole cell of *Proteus mirabilis* can be seen at **Figure 5**. Although the flagella from whole living bacteria may be longer than the isolated flagella, the repeating structure of the flagella is exactly the same in all cases. Therefore, the as prepared MIPs-receptors might be candidates to bind with *Proteus mirabilis* (PM), which could be termed as epitope imprinting for the detection of the target.

As such, the sensors were assessed in the presence of the whole cell of *Proteus mirabilis* (PM) instead of only the flagella (**Figure S3** Supplementary Information). The results indicated that both MIP and NIP-based sensors had no affinity towards PM, up to 15×10^6 CFU/mL. However, at higher concentration values (31×10^6 CFU/mL to 151×10^6 CFU/mL) both sensors showed response towards the cells, but the change of the EMF value was low (MIP 1.71 mV and NIP 1.19 mV). This was probably due to several factors, which included mass transfer effect because of the large size of bacteria and the mobility of cell due to the flagella, which may hamper the electrostatic binding of the cell to the MIP. Moreover, it may also indicate a lack of expression of flagella by bacteria and/or a complex structure at outer surface of bacteria, including addition the aggregation of flagellar filament and hence further optimization is needed. Thus, although it was evident that the MIP material responded to FPM, its use in direct detection of the bacteria may turn out difficult. This could be improved by limiting the mobility of the cell in the sample and/or by addition some transducer element (such as carbon nanotubes or graphene) that could be incorporated into the MIP structure to enhance the transduction characteristic of MIP in order to detect the biorecognition event between the bacteria and the MIP.

5. Conclusions

Potentiometric sensing is highly effective for detecting small molecules; however, it faces challenges when applied to large molecules like proteins and that is more challenges if the structure of the protein is rod-like shape. In addition, the imprinting of such rod-shaped proteins molecules using molecularly imprinted polymers (MIPs) can be difficult. To overcome these

challenges herein, as a proof-of-concept, potentiometric detection of rod-shape *Proteus mirabilis* flagella and its whole cells was first time explored to develop cocktail-free, regenerable biosensors using MIP-based artificial receptors. This approach is a similar process of fabrication of potentiometric ISEs (ion-selective membrane compared to molecularly imprinted polymers), which ISEs cannot be used in the detection of large targets such as proteins or microorganisms. Herein, we were able to detect rod-shaped flagella up to **sub-microgram per milliliter (sub-µg/mL) level** but the sensors suffer from nonspecific adsorption of flagella. Interestingly, the MIP sensor exhibited good selectivity against various non-target proteins which may be attributed to the specific imprinting sites within the polymer matrix and the charge variations among different proteins. While attempts to detect whole cells of *Proteus mirabilis* were limited, further optimization efforts aim to overcome challenges associated with their complex structure, paving the way for enhanced biosensor performance with a significant advancement toward rapid, cost-effective, and portable bacterial detection and integrating MIP-based sensors into real-world food safety and environmental monitoring systems.

Acknowledgments: The URV team would like to acknowledge the financial support from the Spanish ministry of Science, Innovation and Universities (MICIU), the State Research Agency (AEI) and the European Regional Development Fund (ERDF), EU: PID2022-136649OB-I00, PID2019-106862RB-I00/AEI/10.13039/501100011033, PDC2021-120921-I00. The Portuguese Science and Technology Foundation is acknowledged for the financial support of UID/00285, the Centre for Mechanical Engineering, Materials and Processes and LA/P/0112/2020.

References

[1] S. Akter, M.A. Rahman, M. Ashrafudoulla, S.H. Park, S.-D. Ha, Seafood and biofilm: Mitigation strategies for food safety, Food Control. 168 (2025) 110932. https://doi.org/https://doi.org/10.1016/j.foodcont.2024.110932.

[2] W.Q. Ma, Y.Y. Han, L. Zhou, W.Q. Peng, L.Y. Mao, X. Yang, Q. Wang, T.J. Zhang, H.N. Wang, C.W. Lei, Contamination of Proteus mirabilis harbouring various clinically important antimicrobial resistance genes in retail meat and aquatic products from food markets in China, Front. Microbiol. 13 (2022). https://doi.org/10.3389/fmicb.2022.1086800.

[3] A.N. Mafe, G.I. Edo, R.S. Makia, O.A. Joshua, P.O. Akpoghelie, T.S. Gaaz, A.N. Jikah, E. Yousif, E.F. Isoje, U.A. Igbuku, D.S. Ahmed, A.E.A. Essaghah, H. Umar, A review on food spoilage mechanisms, food borne diseases and commercial aspects of food preservation and processing, Food Chem. Adv. 5 (2024) 100852. https://doi.org/10.1016/j.focha.2024.100852.

[4] Y. Wang, S. Zhang, J. Yu, H. Zhang, Z. Yuan, Y. Sun, L. Zhang, Y. Zhu, H. Song, An outbreak of Proteus mirabilis food poisoning associated with eating stewed pork balls in brown sauce, Beijing, Food Control. 21 (2010) 302–305. https://doi.org/https://doi.org/10.1016/j.foodcont.2009.06.009.

[5] D. Drzewiecka, Significance and Roles of Proteus spp. Bacteria in Natural Environments, Microb. Ecol. 72 (2016) 741–758. https://doi.org/10.1007/s00248-015-0720-6.

[6] S. Hameed, L. Xie, Y. Ying, Conventional and emerging detection techniques for pathogenic bacteria in food science: A review, Trends Food Sci. Technol. 81 (2018) 61–73. https://doi.org/https://doi.org/10.1016/j.tifs.2018.05.020.

[7] M.A. Khaleque, S.I. Hossain, M.R. Ali, M. Aly Saad Aly, H.S. Abuelmakarem, M.S. Al Mamun, M.Z. Hossain Khan, Bioreceptor modified electrochemical biosensors for the detection of life threating pathogenic bacteria: a review, RSC Adv. 14 (2024) 28487–28515. https://doi.org/10.1039/d4ra04038d.

[8] X. Xu, X. Lin, L. Wang, Y. Ma, T. Sun, X. Bian, A Novel Dual Bacteria-Imprinted Polymer Sensor for Highly Selective and Rapid Detection of Pathogenic Bacteria, Biosensors. 13 (2023). https://doi.org/10.3390/bios13090868.

[9] Y. Wang, J.K. Salazar, Culture-Independent Rapid Detection Methods for Bacterial Pathogens and Toxins in Food Matrices, Compr. Rev. Food Sci. Food Saf. 15 (2016) 183–205. https://doi.org/10.1111/1541-4337.12175.

[10] C. Johnson, C. Marquez, D. Olson, T. Ward, S. Cheney, T. Hulten, T. Ton, C.R. Webb, J. Dunn, Development and Performance Of a Multiplex PCR Assay For the Detection of

Bacteria in Sterile Body Fluids, Future Microbiol. 18 (2023) 187–195. https://doi.org/10.2217/fmb-2022-0226.

[11] C.M. Brown, C. Staley, P. Wang, B. Dalzell, C.L. Chun, M.J. Sadowsky, A High-Throughput DNA-Sequencing Approach for Determining Sources of Fecal Bacteria in a Lake Superior Estuary, Environ. Sci. \& Technol. 51 (2017) 8263–8271. https://doi.org/10.1021/acs.est.7b01353.

[12] M. Smolejová, J. Krčmáriková, I. Cihová, P. Sulo, Are ELISA and PCR Discrepancies in the Identification of Chlamydia pneumoniae Caused by the Presence of "Chlamydia-Related Bacteria"?, Microorganisms. 11 (2023). https://doi.org/10.3390/microorganisms11010187.

[13] R.C. Nnachi, N. Sui, B. Ke, Z. Luo, N. Bhalla, D. He, Z. Yang, Biosensors for rapid detection of bacterial pathogens in water, food and environment, Environ. Int. 166 (2022) 107357. https://doi.org/https://doi.org/10.1016/j.envint.2022.107357.

[14] D. Ivnitski, I. Abdel-Hamid, P. Atanasov, E. Wilkins, Biosensors for detection of pathogenic bacteria, Biosens. Bioelectron. 14 (1999) 599–624. https://doi.org/https://doi.org/10.1016/S0956-5663(99)00039-1.

[15] S. Bazsefidpar, C. Saweres-Argüelles, G. Gutiérrez, M. Matos, V. Calero, E. Serrano-Pertierra, P. García, M. del Carmen Blanco-López, Biomolecules for early detection of biofilms through point-of-use devices, Microchem. J. 207 (2024) 111702. https://doi.org/https://doi.org/10.1016/j.microc.2024.111702.

[16] M. Alizadeh Sani, W. Zhang, A. Abedini, A. Khezerlou, N. Shariatifar, E. Assadpour, F. Zhang, S.M. Jafari, Intelligent packaging systems for the quality and safety monitoring of meat products: From lab scale to industrialization, Food Control. 160 (2024) 110359. https://doi.org/https://doi.org/10.1016/j.foodcont.2024.110359.

[17] S. Radhakrishnan, S. Lakshmy, S. Santhosh, N. Kalarikkal, B. Chakraborty, C.S. Rout, Recent Developments and Future Perspective on Electrochemical Glucose Sensors Based on 2D Materials, Biosensors. 12 (2022). https://doi.org/10.3390/bios12070467.

[18] A. Ko, C. Liao, Paper-based colorimetric sensors for point-of-care testing, Anal. Methods. 15 (2023) 4377–4404. https://doi.org/10.1039/D3AY00943B.

[19] C.-Y. Hsu, J.A. Rizaev, H. Pallathadka, S. Mansouri, D.O. Bokov, S. Sharma, G. Rathore, P. Rajput, Y.F. Mustafa, M.K. Abosaoda, A review of new emerging biosensors based on

bacteria-imprinted polymers towards pathogenic bacteria: Promising new tools for selective detection, Microchem. J. 207 (2024) 111918. https://doi.org/https://doi.org/10.1016/j.microc.2024.111918.

[20] Y. Saylan, S. Kılıç, A. Denizli, Biosensing Applications of Molecularly Imprinted-Polymer-Based Nanomaterials, Processes. 12 (2024). https://doi.org/10.3390/pr12010177.

[21] R.A. Hassan, S. Abu Hanifah, L.Y. Heng, Advancements and prospects of molecularly imprinted polymers as chemical sensors: A comprehensive review, Talanta. 287 (2025) 127592. https://doi.org/https://doi.org/10.1016/j.talanta.2025.127592.

[22] J.J. BelBruno, Molecularly Imprinted Polymers, Chem. Rev. 119 (2019) 94–119. https://doi.org/10.1021/acs.chemrev.8b00171.

[23] Y. Li, L. Luo, Y. Kong, Y. Li, Q. Wang, M. Wang, Y. Li, A. Davenport, B. Li, Recent advances in molecularly imprinted polymer-based electrochemical sensors, Biosens. Bioelectron. 249 (2024) 116018. https://doi.org/https://doi.org/10.1016/j.bios.2024.116018.

[24] R.D. Crapnell, N.C. Dempsey-Hibbert, M. Peeters, A. Tridente, C.E. Banks, Molecularly imprinted polymer based electrochemical biosensors: Overcoming the challenges of detecting vital biomarkers and speeding up diagnosis, Talanta Open. 2 (2020) 100018. https://doi.org/https://doi.org/10.1016/j.talo.2020.100018.

[25] L. Wu, X. Li, H. Miao, J. Xu, G. Pan, State of the art in development of molecularly imprinted biosensors, View. 3 (2022) 1–13. https://doi.org/10.1002/VIW.20200170.

[26] G. Vasapollo, R. Del Sole, L. Mergola, M.R. Lazzoi, A. Scardino, S. Scorrano, G. Mele, Molecularly imprinted polymers: Present and future prospective, Int. J. Mol. Sci. 12 (2011) 5908–5945. https://doi.org/10.3390/ijms12095908.

[27] X.Y. Zhuang, C.J. Lo, Construction and loss of bacterial flagellar filaments, Biomolecules. 10 (2020) 1–14. https://doi.org/10.3390/biom10111528.

[28] X.Y. Zhuang, S. Guo, Z. Li, Z. Zhao, S. Kojima, M. Homma, P. Wang, C.J. Lo, F. Bai, Live-cell fluorescence imaging reveals dynamic production and loss of bacterial flagella, Mol. Microbiol. 114 (2020) 279–291. https://doi.org/10.1111/mmi.14511.

[29] H. Kodaka, A.Y. Armfield, G.L. Lombard, V.R. Dowell, Practical procedure for demonstrating bacterial flagella, J. Clin. Microbiol. 16 (1982) 948–952. https://doi.org/10.1128/jcm.16.5.948-952.1982.

[30] M.A.R. Khan, A.R. Aires Cardoso, M.G.F. Sales, S. Merino, J.M. Tomás, F.X. Rius, J. Riu, Artificial receptors for the electrochemical detection of bacterial flagellar filaments from Proteus mirabilis, Sensors Actuators, B Chem. 244 (2017) 732–741. https://doi.org/10.1016/j.snb.2017.01.018.

[31] G. Pilvenyte, V. Ratautaite, R. Boguzaite, S. Ramanavicius, C.F. Chen, R. Viter, A. Ramanavicius, Molecularly Imprinted Polymer-Based Electrochemical Sensors for the Diagnosis of Infectious Diseases, Biosensors. 13 (2023) 1–28. https://doi.org/10.3390/bios13060620.

[32] S. Ramanavičius, I. Morkvėnaitė-Vilkončienė, U. Samukaitė-Bubnienė, V. Ratautaitė, I. Plikusienė, R. Viter, A. Ramanavičius, Electrochemically Deposited Molecularly Imprinted Polymer-Based Sensors, Sensors. 22 (2022). https://doi.org/10.3390/s22031282.

[33] S. Ramanavicius, A. Ramanavicius, Conducting polymers in the design of biosensors and biofuel cells, Polymers (Basel). 13 (2021) 1–19. https://doi.org/10.3390/polym13010049.

[34] S. Ramanavicius, A. Jagminas, A. Ramanavicius, Advances in molecularly imprinted polymers based affinity sensors (review), Polymers (Basel). 13 (2021). https://doi.org/10.3390/polym13060974.

[35] M.A.R. Khan, Plastic antibody for the detection of bacterial proteins and microorganisms, PhD Thesis, Universitat Rovira i Virgili, Tarragona, Spain, Oct. 21, 2016. (n.d.). http://www.tdx.cat/handle/10803/397674.

[36] C.X. Chen, S.L. Mu, The electrochemical preparation of polyphenol with conductibility, Chinese J. Polym. Sci. (English Ed. 20 (2002) 309–316.

[37] A.L. Pang, A. Arsad, M. Ahmadipour, Synthesis and factor affecting on the conductivity of polypyrrole: a short review, Polym. Adv. Technol. 32 (2021) 1428–1454. https://doi.org/10.1002/pat.5201.

[38] Y. Xie, X. He, R. Yu, Y. Jin, L. Tan, Portable pH meter-based competitive immunoassay of E-selectin using urease-encapsulated metal-organic frameworks, Talanta. 287 (2025) 127613. https://doi.org/https://doi.org/10.1016/j.talanta.2025.127613.

[39] M.F. Frasco, L.A.A.N.A. Truta, M.G.F. Sales, F.T.C. Moreira, Imprinting technology in electrochemical biomimetic sensors, Sensors (Switzerland). 17 (2017). https://doi.org/10.3390/s17030523.

[40] S.A.A. Almeida, L.A.A.N.A. Truta, R.B. Queirós, M.C.B.S.M. Montenegro, A.L. Cunha,

M.G.F. Sales, Optimizing potentiometric ionophore and electrode design for environmental on-site control of antibiotic drugs: application to sulfamethoxazole., Biosens. Bioelectron. 35 (2012) 319–26. https://doi.org/10.1016/j.bios.2012.03.007.

[41] T.S.C.R. Rebelo, C. Santos, J. Costa-Rodrigues, M.H. Fernandes, J.P. Noronha, M.G.F. Sales, Novel prostate specific antigen plastic antibody designed with charged binding sites for an improved protein binding and its application in a biosensor of potentiometric transduction, Electrochim. Acta. 132 (2014) 142–150. https://doi.org/10.1016/j.electacta.2014.03.108.

[42] R.L. Solsky, Ion-selective electrodes, Anal. Chem. 62 (1990) 21R-33R. https://doi.org/10.1021/ac00211a011.

[43] G. Ruiz, N. Ryan, K. Rutschke, O. Awotunde, J.D. Driskell, Antibodies Irreversibly Adsorb to Gold Nanoparticles and Resist Displacement by Common Blood Proteins, Langmuir. 35 (2019) 10601–10609. https://doi.org/10.1021/acs.langmuir.9b01900.

[44] Y. Sood, K. Singh, H. Mudila, P.E. Lokhande, L. Singh, D. Kumar, A. Kumar, N.M. Mubarak, M.H. Dehghani, Insights into properties, synthesis and emerging applications of polypyrrole-based composites, and future prospective: A review, Heliyon. 10 (2024) e33643. https://doi.org/10.1016/j.heliyon.2024.e33643.

[45] M. Zhou, J. Heinze, Electropolymerization of pyrrole and electrochemical study of polypyrrole: 1. Evidence for structural diversity of polypyrrole, Electrochim. Acta. 44 (1999) 1733–1748. https://doi.org/https://doi.org/10.1016/S0013-4686(98)00293-X.

[46] M.A. Panagopoulou, D. V Stergiou, I.G. Roussis, M.I. Prodromidis, Impedimetric biosensor for the assessment of the clotting activity of rennet, Anal. Chem. 82 (2010) 8629–8636.

[47] I.I. Suni, Impedance methods for electrochemical sensors using nanomaterials, TrAC Trends Anal. Chem. 27 (2008) 604–611. https://doi.org/https://doi.org/10.1016/j.trac.2008.03.012.

[48] J.S. Daniels, Label-free impedance biosensors: opportunities and challenges, Electroanalysis. 19 (2008) 1239–1257.

[49] S.-J. Ding, B.-W. Chang, C.-C. Wu, M.-F. Lai, H.-C. Chang, Impedance spectral studies of self-assembly of alkanethiols with different chain lengths using different immobilization strategies on Au electrodes, Anal. Chim. Acta. 554 (2005) 43–51.

https://doi.org/https://doi.org/10.1016/j.aca.2005.08.046.

[50] S.-J. Ding, B.-W. Chang, C.-C. Wu, M.-F. Lai, H.-C. Chang, Electrochemical evaluation of avidin–biotin interaction on self-assembled gold electrodes, Electrochim. Acta. 50 (2005) 3660–3666. https://doi.org/https://doi.org/10.1016/j.electacta.2005.01.011.

[51] T.S.C.R. Rebelo, C. Santos, J. Costa-Rodrigues, M.H. Fernandes, J.P. Noronha, M.G.F. Sales, Novel Prostate Specific Antigen plastic antibody designed with charged binding sites for an improved protein binding and its application in a biosensor of potentiometric transduction, Electrochim. Acta. 132 (2014) 142–150. https://doi.org/10.1016/j.electacta.2014.03.108.

[52] R.P. Buck, E. Lindner, Recomendations for nomenclature of ion-selective electrodes (IUPAC recommendations 1994), Pure Appl. Chem. 66 (1994) 2527–2536. https://doi.org/10.1351/pac199466122527.

Figure captions

Figure 1. Schematic representation of the fabrication of the biosensor. (A) working electrode of the Au-SPE, (B) deposition of Flagella from *Proteus mirabilis* (FPM); (C) electropolymerization of pyrrole on the surface containing deposited FPM; (D) binding sites formed after removal of FPM entrapped in the polymeric network by trypsin action.

Figure 2. Consecutive cyclic voltammograms (A) obtained by 15 CV cycles in pyrrole solutions prepared in acetate buffer and in electrodes previously incubated in FPM solutions prepared in MES buffer (MIP) or in MES buffer (control, NIP) - along the corresponding surface blocking test (B) obtained by CV in 5.0 mM $[Fe(CN)_6]^{3-}$ and 5.0 mM $[Fe(CN)_6]^{4-}$, in MES buffer pH 5, of MIP and NIP electrodes, after the polymer formation, compared to the reading of a cleaned electrode; Nyquist plots in EIS (C) and SWV voltammograms (D) of the clean Au-SPE electrodes and the MIP or NIP-films, as-grown on the electrode, before and after template removal. Data obtained in 5.0 mM $[Fe(CN)_6]^{3-}$ and 5.0 mM $[Fe(CN)_6]^{4-}$ in MES buffer pH 5.

Figure 3. EMF readings plotted against time after an initial stabilization period, obtained for consecutive increasing concentrations of FPM with MIP and NIP sensors (A), and the corresponding calibration curves (n = 3) in HEPES buffer pH 7.3 (B).

Figure 4. Selectivity study of the MIPs and NIPs-based sensors followed by the normalized response of FPM and interfering model proteins such as BSA, PA, GOx.

Figure 5. TEM images of whole cell of PM with high (A) and low (B) magnification: length of PM ≈ 3 μm and width ≈ 2μm. The curve lines represent the flagella at the outer surface of PM.

Figure 1

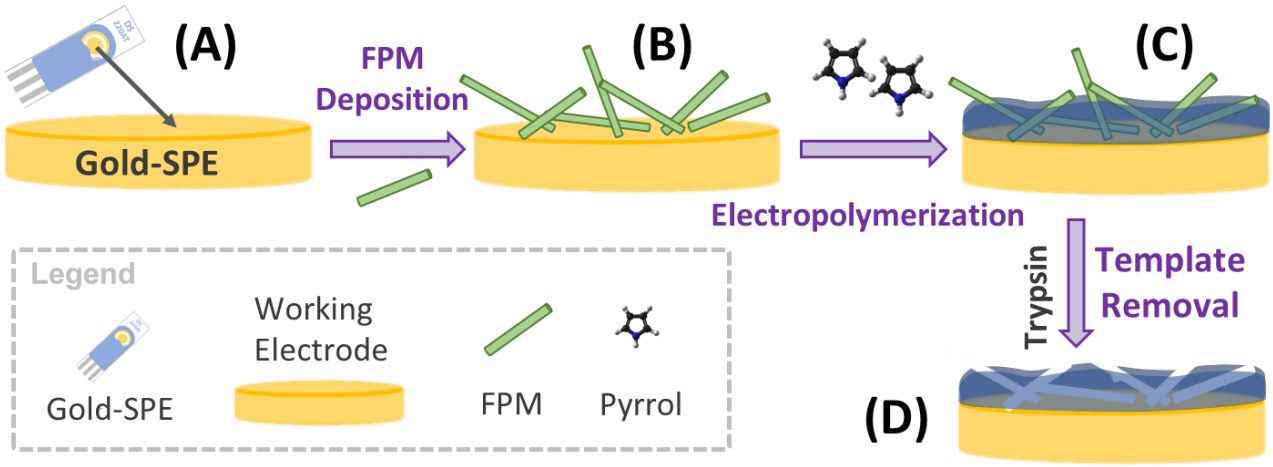

Figure 2

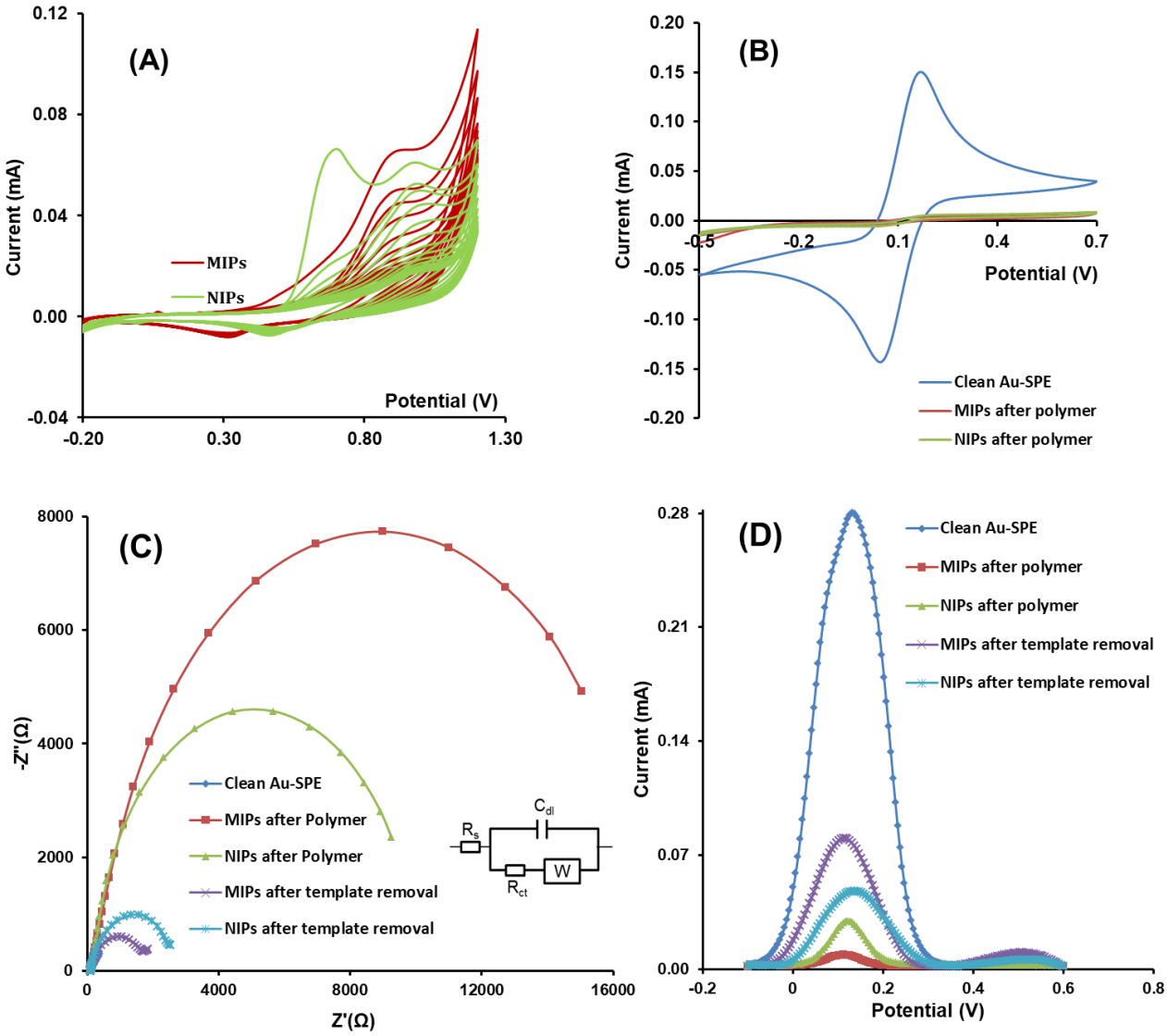
(A)
Current (mA)
Potential (V)
MIPs
NIPs
(B)
Current (mA)
Potential (V)
Clean Au-SPE
MIPs after polymer
NIPs after polymer
(C)
-Z''(Ω)
Z'(Ω)
Clean Au-SPE
MIPs after Polymer
NIPs after Polymer
MIPs after template removal
NIPs after template removal
Cdl
Rs
W
Rct
(D)
Current (mA)
Potential (V)
Clean Au-SPE
MIPs after polymer
NIPs after polymer
MIPs after template removal
NIPs after template removal

Figure 3

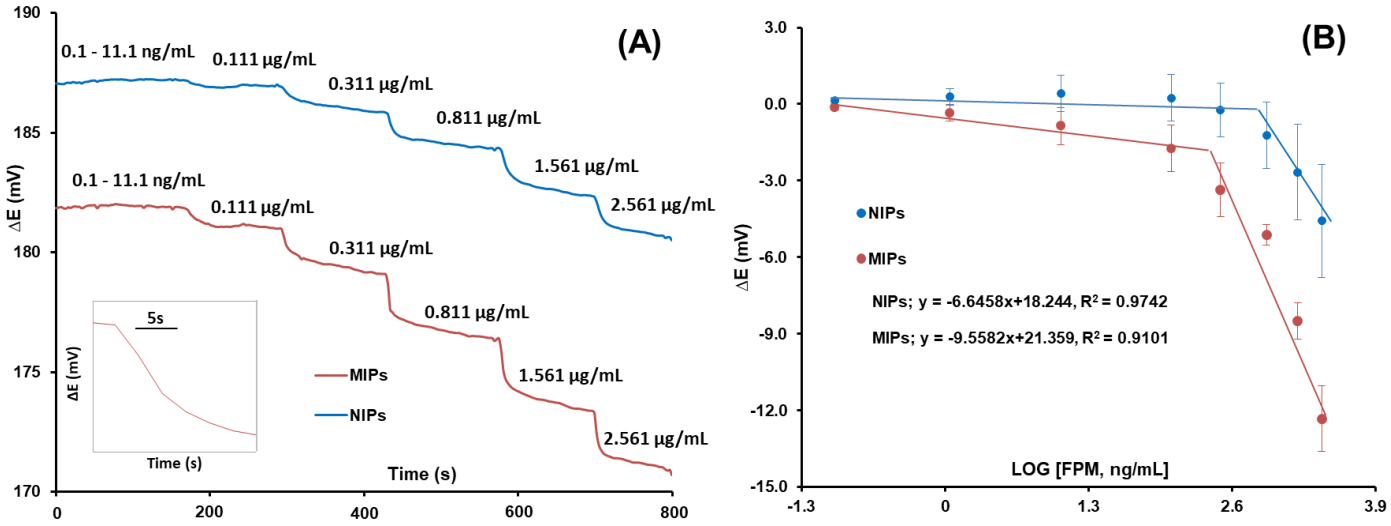
(A)
0.1 - 11.1 ng/mL
0.111 µg/mL
0.311 µg/mL
0.811 µg/mL
1.561 µg/mL
2.561 µg/mL
0.1 - 11.1 ng/mL
0.111 µg/mL
0.311 µg/mL
0.811 µg/mL
1.561 µg/mL
2.561 µg/mL
5s
ΔE (mV)
Time (s)
MIPs
NIPs
ΔE (mV)
Time (s)
190
185
180
175
170
0
200
400
600
800
(B)
NIPs
MIPs
NIPs; y = -6.6458x+18.244, R² = 0.9742
MIPs; y = -9.5582x+21.359, R² = 0.9101
ΔE (mV)
LOG [FPM, ng/mL]
3.0
0.0
-3.0
-6.0
-9.0
-12.0
-15.0
-1.3
0
1.3
2.6
3.9

Figure 4

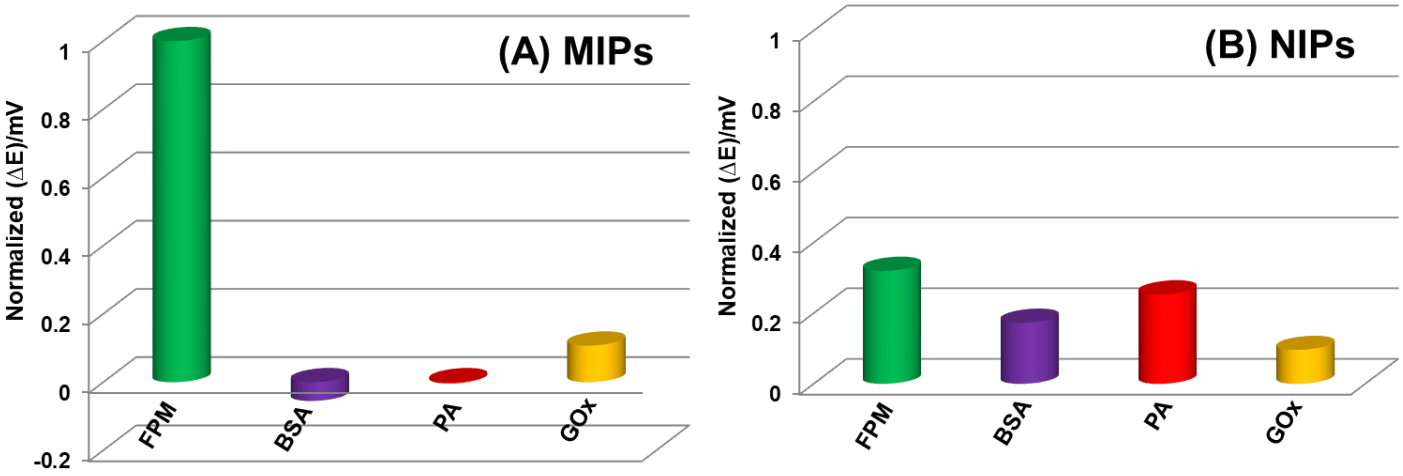
(A) MIPs
Normalized (ΔE)/mV
1
0.8
0.6
0.4
0.2
0
-0.2
FPM
BSA
PA
GOx
(B) NIPs
Normalized (ΔE)/mV
1
0.8
0.6
0.4
0.2
0
FPM
BSA
PA
GOx

Figure 5

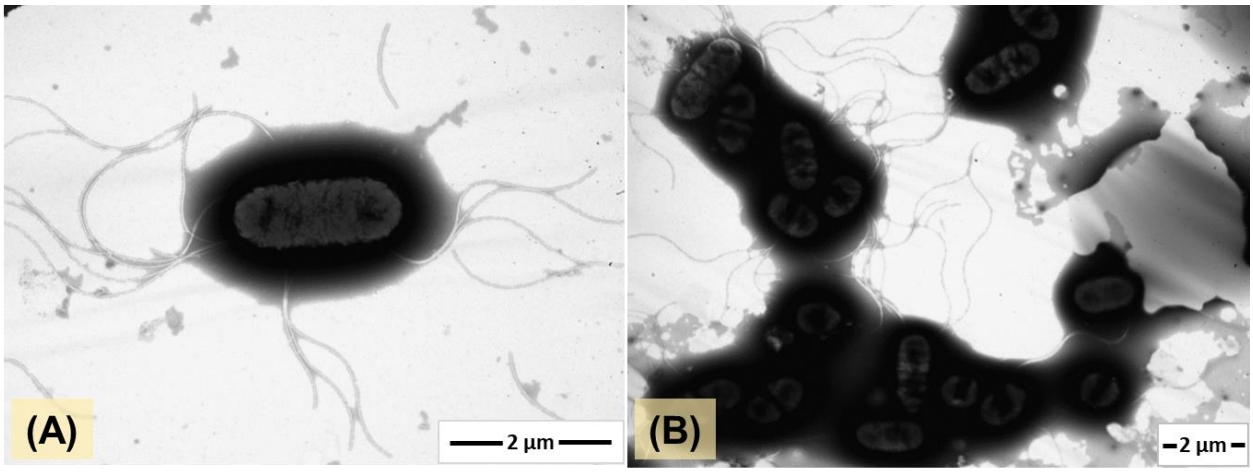
(A)
2 µm
(B)
2 µm